Vortex ratchet effects in films with a periodic array of antidots

Clécio C. de Souza Silva,[1,*] J. Van de Vondel,[1] B. Y. Zhu,[2,†] M. Morelle,[1] and V. V. Moshchalkov[1,‡]
[1]*INPAC - Institute for Nanoscale Physics and Chemistry, Nanoscale Superconductivity and Magnetism Group, Katholieke Universiteit Leuven, Celestijnenlaan 200 D, B-3001 Leuven, Belgium*
[2]*Quantum Phenomena Observation Technology Laboratory, The Institute of Physical and Chemical Research (RIKEN) and Advanced Research Laboratory Hitachi Ltd. Hatoyama, Saitama 350-0395, Japan*
(Received 23 March 2005; revised manuscript received 25 October 2005; published 9 January 2006)

The vortex ratchet effect has been studied in Al films patterned with square arrays of submicron antidots. We have investigated the transport properties of two sets of samples: (i) asymmetrical antidots where vortices are driven by an unbiased ac current and (ii) symmetrical antidots where in addition to the ac drive a dc bias was used. For each sample, the rectified dc voltage is measured as a function of drive amplitude and frequency, magnetic field, and temperature. As unambiguously shown by our data, the voltage rectification in the asymmetric antidots is induced by the intrinsic asymmetry in the pinning potential created by the antidots, whereas the rectification in the symmetric antidots is induced by the dc bias. In addition, the experiments reveal interesting collective phenomena in the vortex ratchet effect. At fields below the first matching field (H_1), the dc-voltage-ac-drive characteristics present two rectification peaks, which is interpreted as an interplay between the one-dimensional motion of weakly pinned incommensurate vortex rows and the two-dimensional motion of the whole vortex lattice. We also discuss the different dynamical regimes controlling the motion of interstitial and trapped vortices at fields higher than H_1 and their implications for the vortex ratchet effect.

DOI: 10.1103/PhysRevB.73.014507 PACS number(s): 74.78.Na, 74.40.+k, 05.40.−a, 85.25.−j

I. INTRODUCTION

Ratchets are systems with an asymmetric periodic potential capable of promoting unidirectional transport of classical or quantum objects subject to an unbiased fluctuating drive. For that purpose, the external forcing must be a nonequilibrium one, like an alternating force or a colored noise, since useful work cannot be extracted from equilibrium fluctuations only. The ratchet effect was first used to explain biochemical mechanisms such as the intracellular transport of macromolecules.[1] Since then, parallel to advances in the theoretical understanding,[2] several devices have been proposed and fabricated in order to test the ratchet idea at the classical and quantum levels and to use the ratchet effect for particle segregation and motion rectification of electrons and fluxons.[3] Most of this work, however, is focused on ratchet systems consisting of single objects or an assembly of weakly interacting objects. Much less is known about the collective rectification of strongly interacting systems via the ratchet effect, and work on this subject carried out so far is mostly theoretical.

Vortices in superconductors with a periodic array of pinning centers have proven to be an ideal system in which to study collective dynamical phenomena of particles moving in a periodic potential. Several interesting dynamical effects have already been studied in these systems. For instance, as demonstrated theoretically[4] and experimentally,[5–7] periodic pinning potentials are able to guide vortex motion into high-symmetry directions of the pinning lattice. Another remarkable dynamical effect in these systems is the presence of Shapiro steps in the voltage-current characteristics when an rf current is coupled to the dc drive.[8] The steps appear due to phase locking between the rf signal and the vortex motion over the periodic pining structure.

Controllable motion of vortices by means of the ratchet effect was recently demonstrated in experiments performed on superconducting samples with periodic arrays of asymmetric pinning centers[9,10] and for asymmetric configurations of symmetrical pinning sites.[7] These structures are able to break the symmetry of the vortex pinning potential and to promote vortex motion rectification when an unbiased ac current is applied. In Ref. 9, for instance, the vortex ratchet effect was demonstrated in a Nb film where the asymmetrical pinning potential was given by an array of triangular magnetic dots. In Ref. 10, we observed pronounced rectification effects in Al films where the symmetry of the pinning potential was broken by engineering a composite configuration of antidot lattices with big and small antidots placed close to each other.

Despite a great deal of theoretical efforts[11–15] aimed at the description of the ratchet dynamics of vortices in asymmetrical pinning potentials, these systems are still quite far from being completely understood. The vortex motion itself, in the presence of strong pinning sites, is still a subject of intense study. Differently from many other systems, vortices are soft objects; their core is able to deform to better adjust to the available pinning potential. Due to this property, the usual approximation of treating vortices as localized overdamped particles may break down and the resulting vortex ratchet effect can be quite different from, for instance, the effects known for overdamped Brownian ratchets. Indeed, as we have recently shown, the dynamics ruling the voltage rectification in a superconducting film with an array of asymmetrical antidots can be described by underdamped equations of motion.[10] This means that this system can be regarded as an example of *inertia ratchet* systems, even though the true mass of a vortex is negligible.

In the present paper, we investigate in detail vortex motion rectification in Al films with nanoengineered antidot arrays as a function of ac excitation, magnetic field, and temperature. Two systems are investigated: (a) square arrays of

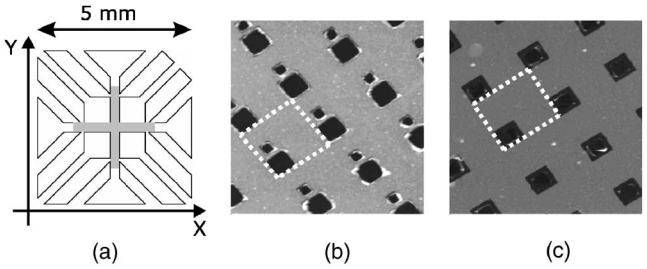

FIG. 1. Layout of the Al samples. (a) Cross- shaped geometry of the samples. AFM images of sample AAD2 (b) and SAD (c). The dashed lines indicate the corresponding unit cell, of size 1.5 $\times 1.5\ \mu m^2$. Big (small) square antidots have side 600 nm (300 nm).

asymmetrical antidots excited by a symmetrical ac current, an intrinsic ratchet system and (b) a square array of *symmetrical* antidots excited by an ac current coupled to a dc bias: i.e., a tilted-potential ratchet. For fields below the first matching field, $H_1=\Phi_0/a_p^2$ (where $\Phi_0=h/2e$ is the flux quantum and a_p is the antidot lattice constant), the vortex response in both systems is characterized by hysteresis, which suggests underdamped motion, and a double rectification peak at some incommensurate fields. These results are interpreted in terms of a minimal inertia ratchet model and molecular dynamics simulations of "inertial" vortices. The simulation results indicate that the double peak observed at incommensurate fields can be explained in terms of plastic deformation of the vortex lattice. For fields higher than H_1, our data reveal that the motion of interstitial vortices is essentially overdamped, in contrast with the unusual underdamped dynamics of the vortices trapped by the antidots. This result suggests that the underlying inertial effect is connected to the strong interaction between the vortices and antidots and not to the real mass of the vortices.

The paper is organized as follows. In Sec. II, we describe the sample preparation, the experimental procedure, and the experimental results. In Sec. III, we present the details of our underdamped model and the molecular dynamics simulations. The experimental data, as well as a comparison between modeling and experiment, are discussed in Sec. IV. Finally, in Sec. V, we draw our conclusions.

II. EXPERIMENTAL RESULTS

A. Sample preparation and experimental details

The experiments were performed on three different Al thin films, thermally evaporated on a SiO_2 substrate patterned by electron beam lithography. For all samples the pattern was designed in a cross-shaped geometry to allow four-point measurements in the two perpendicular directions [see Fig. 1(a)]. The cross consists of two 300-μm-wide strips containing the nanoengineered array (period $a_p=1.5\ \mu$m) of pinning sites. This gives a value of 0.92 mT for the first matching field. The first two samples (AAD1 and AAD2) have the same unit cell consisting of a small ($300\times 300\ nm^2$) and big ($600\times 600\ nm^2$) antidot separated by a thin superconducting wall (90 nm) and approximate thicknesses (38 and 37 nm). The third sample (SAD) has a symmetric unit cell consisting of $600\times 600\ nm^2$ square antidots and a thickness of 22 nm. Figures 1(b) and 1(c) show atomic force micrographs (AFM's) of samples AAD2 and SAD, respectively. The dashed lines depict the unit cell ($1.5\times 1.5\ \mu m^2$) of the respective sample. The white dots observed in the images are particles of resist layer which did not come off during the lift-off procedure. These particles are innocuous to our experiment.

TABLE I. Superconducting parameters for the three samples studied.

	AAD1	AAD2	SAD
Thickness t (nm)	38	37	22
Critical temperature T_c (K)	1.469	1.438	1.532
Mean free path l_e (nm)	3.9	8.1	3.4
Coherence length $\xi(0)$ (nm)	67.5	97	63
Penetration depth $\lambda(0)$ (nm)	195	136	210
GL parameter κ	2.89	1.40	3.32

Table I shows the superconducting parameters for all three samples. The superconducting critical temperature T_c was obtained by using a resistance criterion of 10% of the normal-state resistance in a zero-field measurement. The resistive transition for all samples was sharp, with a width typically of $\Delta T_c \sim 3$ mK. From the residual resistivity at 4.2 K, the electron mean free path l_e was found. From this we have calculated the coherence length $\xi(0)$ and the penetration depth $\lambda(0)$ using the dirty limit expressions. All samples are type-II superconductors; i.e., their Ginzburg-Landau parameter is $\kappa=\lambda(0)/\xi(0)>1/\sqrt{2}$. Note that, although samples AAD1 and AAD2 share the same pattern and have similar thicknesses, their mean free paths were quite different, which is a result of the different evaporating conditions (base pressure and growth rate) in which the samples were prepared.

The transport measurements were performed in a cryostat using ac and/or dc currents applied at the end of the cross legs in the x direction. The magnetic field was applied perpendicularly to the xy plane. In all ac measurements, the applied ac current was a sinusoidal wave—i.e., $I(t)=I_{ac}\sin(2\pi ft)$, where f is the excitation frequency and I_{ac} is its amplitude. The voltage was acquired in four point mode by an oscilloscope, used as an analog-digital converter. The wave form was averaged over several cycles (typically 200–500 cycles) in order to enhance the signal-to-noise ratio. The dc voltage was then obtained by integrating the "clean" wave form.

B. Rectification by unbiased asymmetrical antidots

Figure 2(a) shows a contour plot of the dc voltage across the sample (V_{dc}) as a function of reduced magnetic field (H/H_1) and current amplitude (I_{ac}) at a temperature $T=0.98T_c$ and excitation frequency $f=1$ kHz. At $H=0$, one can observe a clear sign inversion of the dc voltage. Note that the voltage drop due to vortex motion is given by $V_{dc}=L(\langle v\rangle\times B)$, where B is the flux density, $\langle v\rangle$ is the time-

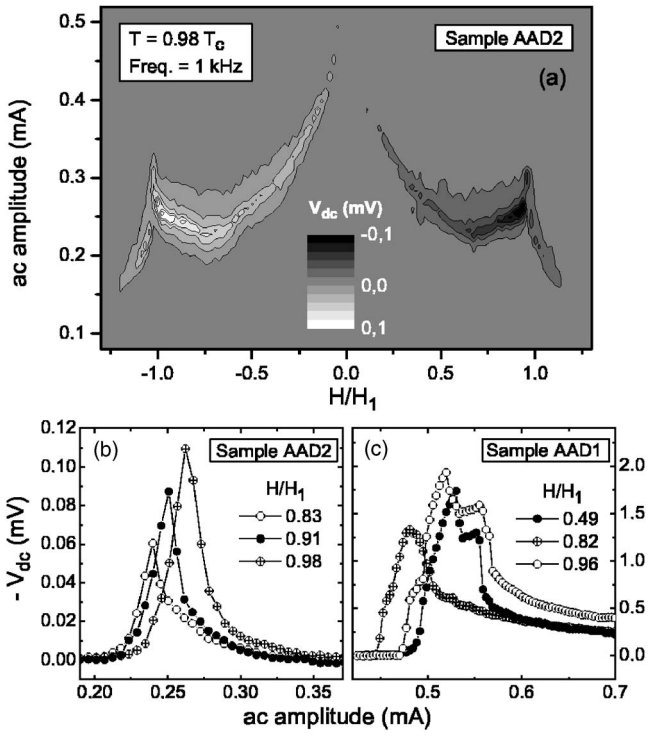

FIG. 2. (a) Contour plot of the dc voltage measured across sample AAD2 as a function of reduced field and ac amplitude at $T=0.98T_c$ and frequency of 1 kHz. (b) Detail of the amplitude dependence of the dc voltage shown in (a) for fields $H/H_1=0.83$, 0.91, and 0.98. (c) ac-drive amplitude dependence of the dc voltage measured across sample AAD1 at $T=0.976T_c$ and $f=1$ kHz for fields $H/H_1=0.49$, 0.82, and 0.96.

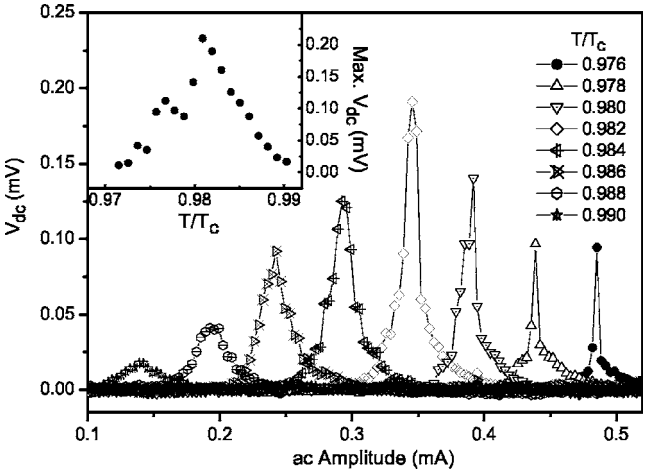

FIG. 3. dc voltage measured across sample AAD2 versus ac amplitude for $H/H_1=0.95$ and $f=1$ kHz at different temperatures, as indicated. Inset: plot of the maximum dc voltage at this field as a function of temperature.

averaged vortex velocity, and L is the distance between the voltage contacts. Thus, the change of V_{dc} sign as H (and, consequently, B) changes its sign means that vortices and antivortices are rectified to the same direction. This simple assumption demonstrates unambiguously the intrinsic rectifying properties of the asymmetrical antidots configuration. A similar behavior of $V_{dc}(H,I_{ac})$ was also observed in sample AAD1, and its plot for the positive field side was presented in Ref. 10. Another important effect demonstrated by Fig. 2(a) is a clear enhancement of the rectified voltage near the first matching field (see also Ref. 10, Fig. 2). This can be explained by the high symmetry of the vortex lattice at this field range which induces coherent, collective vortex motion; that is, all vortices contribute to the rectified voltage in a constructive way.

In panels (b) and (c) of Fig. 2, we show detailed plots of the $V_{dc}-I_{ac}$ characteristics of samples AAD2 and AAD1, respectively. Similarly to single-object ratchet systems, these curves are characterized by a rectification window, in which the rectified voltage increases monotonically, and by the presence of a tail, in which V_{dc} drops smoothly towards zero. The rectification window is defined by two critical forces F_1, where vortices are first depinned to the "easy" ratchet direction, thus marking the onset of voltage rectification, and F_2, for which vortices start moving also to the "harder" direction. At $F=F_2$, the dc rectified voltage has a maximum, since for $F>F_2$ vortices move back and forth in a more and more symmetrical way. For one vortex and in the limit of small thermal noise and frequency, these forces coincide with the two critical depinning forces F_w and F_s of the asymmetric pinning potential (cf. Sec. III).[16] Therefore they determine the effective asymmetry of the pinning potential, which we define here as $\alpha=1-F_1/F_2$. For some field values (usually, for fields close to H_1 or $H_{1/2}$) a second rectification peak is observed, suggesting an interplay between two ratchets (cf. Sec. IV), each having their own critical forces [see Fig. 2(c)]. However, a clear second peak was not identified in the measurements on sample AAD2, which is probably due to a lack of resolution in our measurements in the narrow rectification window of this sample.

By comparing the results obtained on samples AAD1 and AAD2, one can notice the striking difference in the rectified voltage of both samples. For similar reduced temperatures, the maximum dc voltage of AAD2 was several times smaller than that of AAD1. This can be explained by the fact that the coherence length of AAD2 at temperatures close to T_c can be considerably bigger than the antidots [for instance, $\xi_{AAD2}(T=0.97T_c)\simeq 560$ nm]. In this situation, the vortices are not able to resolve the details of the antidots and the effective asymmetry is strongly suppressed. This is clear from the calculation of the asymmetry ratio for both samples at a relatively low temperature $T=0.976T_c$ (where thermal escape can be neglected) and reduced field $H/H_1=0.96$, which gives $\alpha\approx 0.09$ for AAD1 and $\alpha\approx 0.02$ for AAD2.

The coherence length can also play an important role in the temperature dependence of the rectified voltage. In the temperature range we investigated, $\xi(T)$ is typically of the order or bigger than the antidot sizes. In such a situation, the vortex pinning mechanism is mainly given by a local suppression of the order parameter and, thus, the relevant characteristic length of the pinning potential is ξ.[17] Figure 3 shows $V_{dc}-I_{ac}$ characteristics of sample AAD2 at several temperatures for the same reduced field $H/H_1=0.98$. The maximum rectified voltage seems to increase monotonically until a temperature $T\simeq 0.982T_c$, above which it starts to

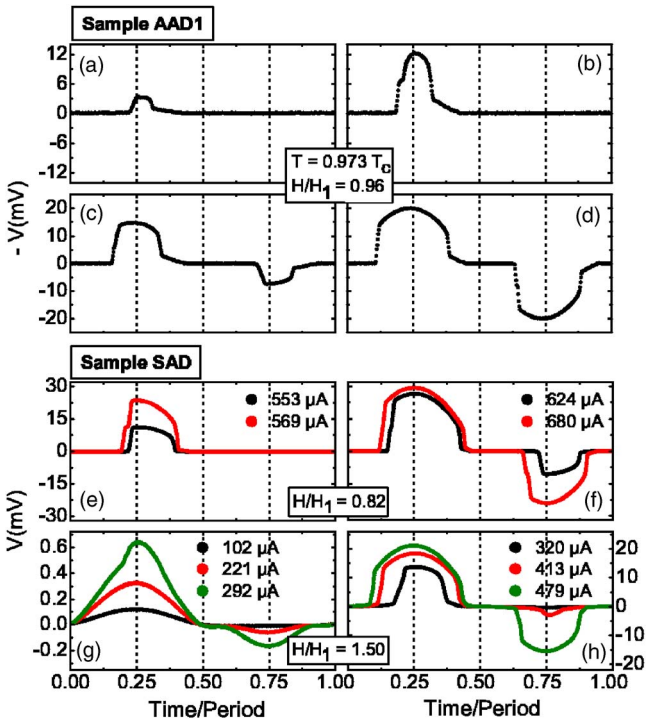

FIG. 4. (Color online) (a)-(d) Time evolution of the voltage output of sample AAD1 at a temperature $T=0.973T_c$, field $H=0.96H_1$, and ac amplitudes $I_{ac}=477$ (a), 502 (b), 544 (c), and 704 μA (d). (e),(f) Voltage output of sample SAD at $T=0.966T_c$, $H=0.82H_1$, a dc bias $I_{dc}=64$ μA, and ac amplitudes $I_{ac}=553$ and 569 μA (e), $I_{ac}=624$ and 680 μA (f). (g),(h) Voltage output of sample SAD at $T=0.966T_c$, $H=1.50H_1$, a dc bias $I_{dc}=64$ μA, and ac amplitudes $I_{ac}=102$, 221, and 292 μA (g), $I_{ac}=320$, 413, and 479 μA (h).

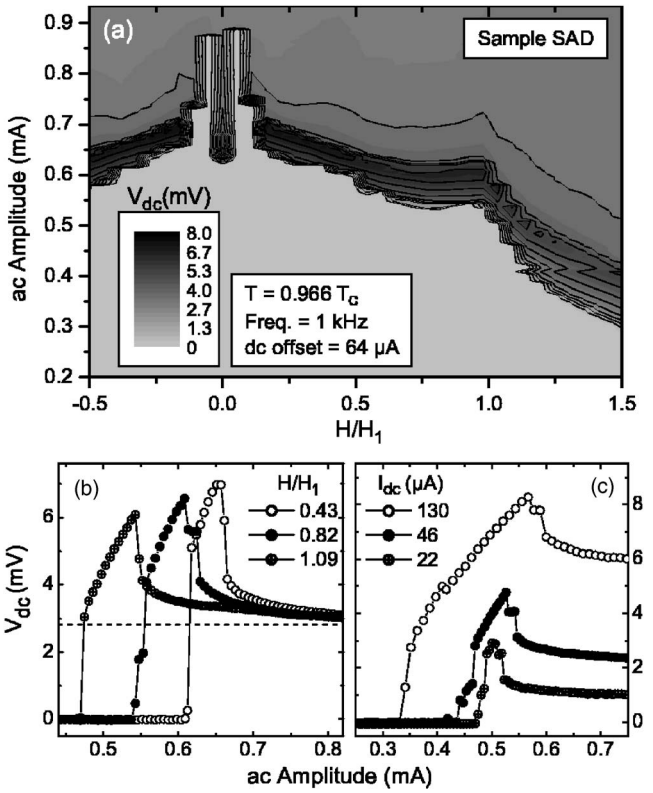

FIG. 5. (a) Contour plot of the dc voltage measured across sample SAD as a function of reduced field and ac amplitude at $T=0.966T_c$, frequency of 1 kHz, and a dc bias of 68 μA. (b) Detail of the amplitude dependence of the dc voltage shown in (a) for fields $H/H_1=0.43$, 0.82, and 1.09. The dashed line indicates the saturation voltage $V_{sat}=R_nI_{dc}=2.8$ mV. (c) ac-drive amplitude dependence of the dc voltage at $T=0.973T_c$, $f=1$ kHz, $H/H_1=0.93$, and different tilts $I_{dc}=130$, 46, and 22 μA.

drop, resulting in a bell-shaped T dependence (see inset). In Brownian ratchets, a decrease in the dc response as the temperature increases is indeed expected.[16] The reason is that, when the Brownian motion of particles is enhanced by thermal noise, more energy is needed to move them in a given direction. However, in the vortex case near the critical temperature, increasing temperature induces not only vortex fluctuations but also a strong increase of the vortex size, which leads to a decrease in the effectiveness of the pinning potential and its asymmetry. At low temperatures, the reduction of fluctuations and vortex size should lead to a monotonic increase in rectification. Nevertheless, when vortices are small enough and their fluctuations are weak, they are more sensitive to the background pinning caused by the natural inhomogeneities of the sample. Due to the disorder induced by the background pinning, the antidot pinning potential may become less effective at lower temperatures, thus causing a reduction of the rectified voltage.

In Figs. 4(a)–4(d) we show the voltage output wave form in one cycle of the ac drive for different drive amplitudes of the $V_{dc}-I_{ac}$ characteristic presented in Fig. 2(c) (open circles). Note that, as discussed above, here negative voltage corresponds to positive vortex velocity, since the applied field is positive. Panels (a) and (b) correspond to points in the rectification window, where the ratchet system behaves as a half-wave rectifier, whereas (c) and (d) correspond to points in the rectification tail. At each half-period of the ac drive, the corresponding half-period of the voltage output in all cases (a-d) is asymmetric; vortices seem to be depinned at a given force and repinned at a lower force value, giving rise to hysteretic behavior. Such a hysteresis was also observed in sample AAD2, but somewhat smoothed due to the strong effects of fluctuations in this sample. As we shall see below, this indicates that the system is ruled by underdamped dynamics.

C. Rectification by dc-biased symmetrical antidots

Since the symmetrical antidot configuration of sample SAD does not produce rectified vortex motion by itself, we externally induce an asymmetry in the system by "tilting" the pinning potential with a small dc current bias. In Fig. 5(a), we show the contour plot of the dc voltage across sample SAD in the $H-I_{ac}$ plane at a temperature $T=0.966T_c$ for a dc bias of $I_{dc}=64$ μA and ac excitations of 1 kHz. [Note that the steps observed in this plot are just artifacts induced by the low resolution of the field sweep (0.05 mT).] In this experiment, no flip of the dc voltage sign is observed. This is indeed expected because here the polarity of a vortex does matter in determining its net velocity. For instance, for a

positive current bias—i.e., in the positive x direction—a vortex with positive polarity experiences a positive slope in the pinning potential (due to the Lorentz force pointing to the negative y direction), whereas an antivortex senses a negative slope. Thus, as the magnetic field changes its sign, so does the asymmetry of the pinning potential in such a way that the cross product $\langle v\rangle \times B$ keeps its sign.

In Fig. 5(b), we present a detailed plot of the $V_{dc}-I_{ac}$ characteristics at fields $H/H_1=0.43$, 0.82, and 1.09, for the experiment of Fig. 5(a). Here, in comparison to the $V_{dc}-I_{ac}$ characteristics of the asymmetric antidot samples (Fig. 2), the important difference is that the rectification tail approaches asymptotically a *finite voltage value*, which depends on the applied dc tilt, whereas the rectification tail of the intrinsically asymmetric samples reaches zero voltage at high ac drives. In the rectification window, however, samples SAD and AAD1 behave in a similar way. For instance, at fields close to H_1, the second rectification peak is also seen in the $V_{dc}-I_{ac}$ curves of sample SAD.

Figure 5(c) presents the rectification effect in sample SAD for different dc biases $I_{dc}=22$, 46, and 130 μA at $H/H_1=0.93$ and $T/T_c=0.973$. At this field, a double-rectification peak is observed for all dc biases. The distance between peaks seems to be constant, whereas the rectification window is wider for higher tilt values. The window is roughly defined by the critical values I_c-I_{dc} and I_c+I_{dc}, where $I_c=501$ μA is the critical depinning current obtained from conventional dc transport measurements. Thus, the system is given an asymmetry of $\alpha=2I_{dc}/(I_c+I_{dc})$. For the tilt $I_{dc}=22$ μA, this amounts to $\alpha\approx 0.086$, which is similar to the intrinsic asymmetry observed in sample AAD1 at $T=0.973T_c$. Another noteworthy point is that the main rectification peak decreases relatively to the saturation voltage for higher tilts. This is consistent with the fact that, in the limit of the critical tilt ($I_{dc}=I_c$), no rectification peak should be observed because there the energy barrier for the easy flow direction disappears completely. In this limiting case, $V_{dc}(I_{ac})$ is expected to grow monotonically from zero to the saturation voltage.

The time evolution of the voltage output for different drive amplitudes of the $V_{dc}-I_{ac}$ characteristics shown in Fig. 5(b) is presented in Figs. 4(e)–4(h). We consider two different fields $H/H_1=0.82$ [(e) and (f)] and 1.50 [(g) and (h)] corresponding, respectively, to the solid circles and crossed circles of Fig. 5(b). In the $H/H_1=0.82$ case, the asymmetrical shape of the half-periods of $V(t)$ resembles that observed in sample AAD1 [shown in panels (a)–(d) of this figure; that is, here a hysteresis in the depinning-repinning process is also observed. The main difference is that in the high-drive limit [panel (f)], the amplitude of the positive half-cycle is higher than the amplitude of the negative one, due to the extrinsic nature of the asymmetry in sample SAD, whereas for sample AAD1 the amplitude of both half-cycles are approximately the same.

For fields higher than H_1 [Figs. 4(g) and 4(h)], there exists an amplitude range for which the voltage half-cycles are symmetrical; that is, no hysteresis is observed. Since this behavior is only present at low ac amplitudes, we can assume that the symmetrical wave forms correspond to motion of interstitial vortices. At $H/H_1=1.5$, the response is strongly enhanced in the positive half-cycle above an amplitude $I_{ac}=292$ μA, suggesting that at this value the vortices trapped by the antidots start moving. The voltage wave form corresponding to this amplitude and above are asymmetrical [panel (h)], resembling the wave forms observed at fields below H_1. A similar evolution of the voltage wave forms as the ac amplitude is varied was also observed in the samples with asymmetrical pinning sites for fields $H>H_1$.

III. THEORETICAL MODELLING

A. Inertia ratchet model

Our experimental data (Fig. 4) clearly demonstrate a pronounced hysteresis in the voltage as a transport current is cycled in both symmetrical and asymmetrical samples. Typical systems exhibiting pronounced hysteresis in their transport properties are driven underdamped particles in periodic potentials. In these systems, the hysteresis in the depinning-repinning process is a consequence of the finite inertial mass of the particles, which has important effects on their transport properties. For instance, in microscopic boundary lubrication problems, the depinning of the (inertial) lubricant particles from the periodic potential of a solid substrate is usually identified as the static friction force whereas the repinning of the particles is identified as the dynamical friction force.[18] Other "inertia" ratchet systems are asymmetrical underdamped Josephson junction arrays[19] and dc superconducting quantum interference devices (SQUID's).[20] In these two examples, the rectified object is the phase of the superconducting order parameter across a junction and the inertia is given by the shunt capacitance of the junctions. This problem is formally the same as that of the mechanical inertia ratchet.

The rectification of inertial particles in a ratchet potential has been studied theoretically by several groups.[19–22] The dynamics of inertia ratchets is more complex than their overdamped counterpart due to the existence of both regular (for moderately underdamped) and chaotic (for extremely underdamped) dynamics. In the regular regime, the amplitude-dependent dc response presents a strong enhancement in the rectification window and a faster decaying tail, as compared to the characteristics of overdamped particles. Inspired by the fact that, in our experiment, (i) the rectified voltage demonstrates hysteretic behavior and (ii) the V_{dc}-I_{ac} characteristic generally has pronounced rectification effect in the rectification window, we propose a description of vortex dynamics in antidot systems in terms of a simplified underdamped model, in which vortices (still treated as particles) are given an apparent mass to account for the observed hysteresis.

We first consider the simpler case of a single vortex in a ratchet potential, here representing the asymmetric antidot array. The equation of motion is given by

$$M\ddot{x} = -\eta\dot{x} - U_p(x) + A\sin(\omega t), \tag{1}$$

where η is the viscous drag coefficient and x is the particle position. The pinning potential $U_p(x)$ is modeled in a simplified way as the double-sine function

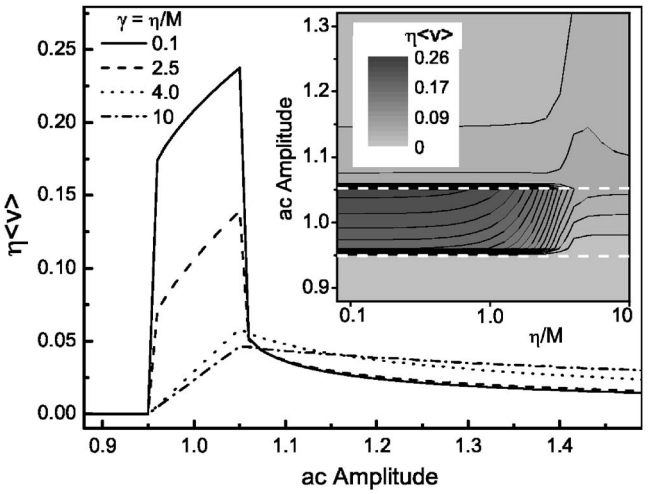

FIG. 6. Time-averaged particle velocity as a function of ac drive amplitude calculated in the single-particle inertia ratchet model [Eq. (1)] for the viscosity-to-mass ratios $\gamma=\eta/M=0.1$, 2.5, 4, and 10 (in units of f_p). Inset: contour plot of average velocity as a function of amplitude and η/M; the dashed lines define the rectification window in this case ($\alpha=0.095$).

$$U_p(x) = -U\left[\sin\left(\frac{2\pi x}{a_p}\right) + \frac{\beta}{2}\sin\left(\frac{4\pi x}{a_p}\right)\right]. \qquad (2)$$

The parameter β defines the asymmetry of the pinning force [$\alpha=2\beta/(1+\beta)$, for $\beta<1/4$], the critical forces being given by $F_w=2\pi(1-\beta)U/a_p$, for a drive along the (weak) positive x direction, and $F_s=2\pi(1+\beta)U/a_p$, for a drive along the (strong) negative x direction. Note that, since here we do not take into account thermal fluctuations, the critical forces which define the rectification window of this system are given deterministically by $F_1=F_w$ and $F_2=F_s$.

The main characteristic frequencies setting the limits of the dynamical regimes of Eq. (1) are the libration frequency in the potential minima, which for $\alpha\lesssim 0.2$ is given approximately by $f_p=\sqrt{U/Ma_p^2}$, and the inverse relaxation time $\gamma=\eta/M$. The quasiadiabatic regime (i.e., close to the zero-frequency adiabatic limit) corresponds to frequencies much smaller than these two characteristic frequencies. In the numerical solution of Eq. (1) we have chosen excitation frequencies $f<10^{-4}f_p$ and $\gamma\geqslant 0.1f_p$, corresponding to the quasiadiabatic regime.

In Fig. 6, we show the net dc velocity versus ac drive amplitude ($\langle v\rangle$-F_{ac} characteristics for different values of γ). Forces are in units of $2\pi U/a_p$ and frequencies (and γ) in units of f_p. For these runs, we have chosen the asymmetry factor $\alpha=0.095$, which is close to the typical values of I_1/I_2 observed in sample AAD1. The inset shows a detailed diagram of $\langle v\rangle$ as a function of A and M. Notice the crossover between the spread rectification in the extreme overdamped limit and the sharp rectification in the extreme underdamped regime. For $\eta/M\gtrsim 4f_p$, the curves are essentially overdamped, following the behavior of the adiabatic solution of a deterministic overdamped ratchet.[10] For $\eta/M\lesssim 2f_p$, the curves are much more pronounced in the rectification window and have a faster decaying tail. We shall compare these results with the experimental data in Sec. IV.

B. Molecular dynamics simulations

Now, we consider the two-dimensional (2D) problem of a lattice of "inertial" vortices interacting with a 2D array of asymmetric pinning sites, which is modeled as two interpenetrating square sublattices of strong and weak attractive potentials. The sublattices have spacing a_p (=1 here) and are shifted with respect to each other by a distance $d=0.2a_p$. All pinning centers are modeled by Gaussian potential wells with a decay length R_p. Hence, the pinning force exerted by the kth pin of one sublattice on the ith vortex reads

$$\mathbf{F}_p^{s,w}(\mathbf{r}_i) = -F_{s,w}\frac{\mathbf{r}_i-\mathbf{R}_k^{s,w}}{R_p}\exp\left(-\left|\frac{\mathbf{r}_i-\mathbf{R}_k^{s,w}}{R_p}\right|^2\right), \qquad (3)$$

where $\mathbf{r}_i$ represents the position of the ith vortex and $\mathbf{R}_k^{s,w}$ is the location of the kth pin of the weak (w) and the strong (s) sublattices, respectively. The intensity of the individual pinning force is denoted by $F_{s,w}$. We define the ratio between the weak and strong pinning forces as $\epsilon=F_w/F_s$. In our simulation, forces (per unit length) are taken in units of $F_0=\Phi_0^2/8\pi^2\Lambda^3$, with Λ the effective superconducting penetration depth. Vortices are considered to interact logarithmically, the corresponding repulsive vortex-vortex force being given by

$$\mathbf{F}_{vv}(\mathbf{r}_i) = F_{vv0}\sum_{j\neq i}^{N_v}\Lambda\hat{\mathbf{r}}_{ij}/|\mathbf{r}_i-\mathbf{r}_j|,$$

where $\hat{\mathbf{r}}_{ij}=(\mathbf{r}_i-\mathbf{r}_j)/|\mathbf{r}_i-\mathbf{r}_j|$. F_{vv0} denotes the strength of the vortex-vortex interaction. The underdamped equation of motion for vortex i is given by

$$M\ddot{\mathbf{r}}_i = \mathbf{F}_L(t) + \mathbf{F}_{vv}(\mathbf{r}_i) + \mathbf{F}_p(\mathbf{r}_i) - \eta\dot{\mathbf{r}}_i. \qquad (4)$$

The ac driving Lorentz force is $\mathbf{F}_L(t)=A\sin(\omega t)$, where $\omega=2\pi/P$ and P is the period of the ac drive. η is the viscosity coefficient and M is the effective mass of an individual vortex. This equation is integrated by molecular dynamics (MD) simulations. Parameters used in the simulations are $R_p=0.13a_0$ and $\Lambda=0.26a_0$. $F_{vv0}=0.06$, $F_{p0}^s=0.5$, and $\epsilon=0.925$, and time step $\tau_0=1/150$. All the frequencies of the ac sine-wave drive are smaller than $10^{-6}/\tau_0$—i.e., into the quasiadiabatic regime. For the mass and viscosity we have chosen, respectively, $M=1$ and $\eta=1$, which, in terms of $f_p=\sqrt{U_p/Ma_p^2}$ (here $U_p=F_sR_p^2/2$ is the amplitude of the individual strong pinning potential), leads to a viscosity-to-mass ratio $\eta/M=2.44f_p$. The MD simulation results will be discussed in the next section.

IV. DISCUSSION

In Fig. 7, we present a fitting of our inertia ratchet model to the experimental data of samples AAD1 and SAD. The data are plotted in normalized units. The normalized critical forces used in the model were the same observed in the respective measurement. In this way, the only adjustable pa-

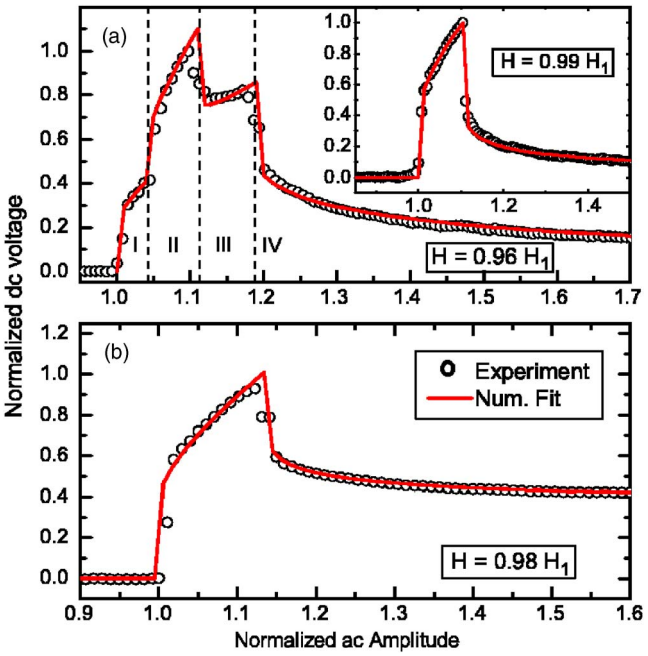

FIG. 7. (Color online) (a) Main frame: normalized dc voltage versus current amplitude (circles) of sample AAD1 at $T=0.973T_c$ and $H=0.96H_1$ and numerical fit obtained from the double ratchet model described in Sec. IV (see also Sec. III) with $\gamma=1.9$ and $\chi=0.5$. The dashed vertical lines define different dynamical regimes of the system (see text). Inset: same as the main frame but with $H=0.99H_1$. The fitting (line) was obtained integrating Eq. (1) with $\gamma=1.8$. (b) Normalized dc voltage versus current amplitude (circles) of sample SAD at $T=0.966T_c$ and $H=0.98H_1$ using an excitation frequency of 1 kHz and a dc bias of 46 μA (which gives a reduced tilt). The fitting (line) was obtained using $\gamma=2.1$.

rameter is the viscosity-to-mass ratio $\gamma=\eta/M$, which is given in units of the libration frequency f_p. For comparison, we have shown in Fig. 6 the V_{dc}-I_{ac} calculated close to the overdamped limit $\gamma=10$. As is clearly seen from this graph, the usual overdamped model fails to describe the ratchet effect of vortices in an antidot lattice, more specifically in our Al samples AAD1 and SAD. On the other hand, the underdamped model with γ values close to the underdamped limit provides very good fitting to our experimental data. For the measurement of sample AAD1 at $T=0.973T_c$ and $H/H_1=0.99$, for example, we used $\alpha=0.095$ (which gives approximately the same normalized critical forces observed in this experiment) and the best fit was obtained with $\gamma=1.8$ [see Fig. 7(a), inset], which is close to the underdamped limit. For the sample SAD at $H/H_1=0.98$ and $T=0.966T_c$, we used $\alpha=0$ (i.e., a symmetrical sinusoidal potential) and added to the driving force a dc component $F_{dc}=0.066F_p$ (where $F_p=2\pi U/a_p$ is the critical force of the pinning potential), in agreement with the I_{dc}/I_p ratio observed in the experiment. In this case the best fit was obtained with $\gamma=2.1$ [Fig. 7(b)].

The success of an underdamped model to describe the voltage induced by vortex motion is not a trivial result. Vortex dynamics is usually treated in terms of overdamped particle models because it is a well-established fact that in most samples the vortex mass is negligible compared to the damping coefficient.[23,24] Nevertheless, these models do not consider the effect of *vortex deformation* that can lead to an irreversibility in the depinning-repinning process and, consequently, to an *apparent inertial effect*. In recent Ginzburg-Landau simulations of a superconductor with an antidot lattice, it was shown that the process of depinning of a vortex from an antidot can be characterized by strong current-induced elongation of the vortex core cross section, which may result in a hysteresis in the pinning mechanism.[25] This effect seems to mimic the behavior of an underdamped particle in a periodic potential and can be responsible for the hysteresis observed in our experiments.

A. Vortex rectification for $H<H_1$

In our experiment, the V_{dc}-I_{ac} curves for some fields below H_1 are characterized by a double-rectification peak. As we pointed out in our previous publication, the second rectification peak can be explained in terms of plastic deformation of the vortex lattice.[10] In other words, the existence of a plastic dynamical phase with a lower critical current gives rise to the appearance of a second ratchet system, which competes with the main ratchet, given by the motion of the whole vortex lattice. The consequences of the existence of two ratchets with different critical forces can be heuristically illustrated by our one-particle underdamped model. Let us consider two independent inertia ratchets. The first one represents the whole vortex lattice, with critical forces F_w and F_s. The second ratchet represents the fraction χ of the vortices that deform plastically and has critical forces $F'_w \leqslant F_w$ and $F'_s \leqslant F_s$. In this way, the total dynamics is simply given by the solution $v(t)$ of the first ratchet for $F(t)>F_w$ and $F(t)<-F_s$, and, otherwise, by the solution $v'(t)$ of the second ratchet, normalized by the factor χ. This simple model provides an excellent fitting to the experimental data for $H<H_1$. For instance, to fit the data of the experiment performed in sample AAD1 at $H=0.96H_1$ and $T/T_c=0.973$, we solved Eq. (1) for both ratchets independently, using for the critical forces the normalized values obtained experimentally, and adjusted the parameters γ and χ. In this case, we obtained $\gamma=1.9$ and $\chi=0.5$ [see Fig. 7(a)].

To get a better insight into how such plastic dynamics can lead to a double peak in the V_{dc}-I_{ac} characteristic, we performed MD simulations of "inertial" vortices for fields $H \leqslant H_1$. The parameters used in the simulations are given in Sec. III B. Figures 8(a)–8(d) show the simulated net velocity of vortices $\langle v \rangle$ as a function of drive amplitude F_{ac} for reduced fields $H/H_1=1$, 0.94, 0.92, and 0.88. The simulations reproduce quite well the double rectification peak observed experimentally. Panels (e) and (f) show the time dependence of the center-of-mass (c.m.) velocity of the vortex lattice at vortex densities $H/H_1=1$ and 0.92, respectively. As in our experiments, here the wave forms of vortex motion during each half-period are asymmetrical—i.e., present hysteretical behavior—which is a result of the finite apparent mass of the vortices. In particular, the simulated wave forms at $H/H_1=0.92$ [panel (f)] evolve similarly to the experimental data of sample AAD1 presented in Figs. 4(a)–4(d). In both experiment and simulations, four different ratchet phases (I–IV) are clearly identified [these phases are defined by vertical dashed

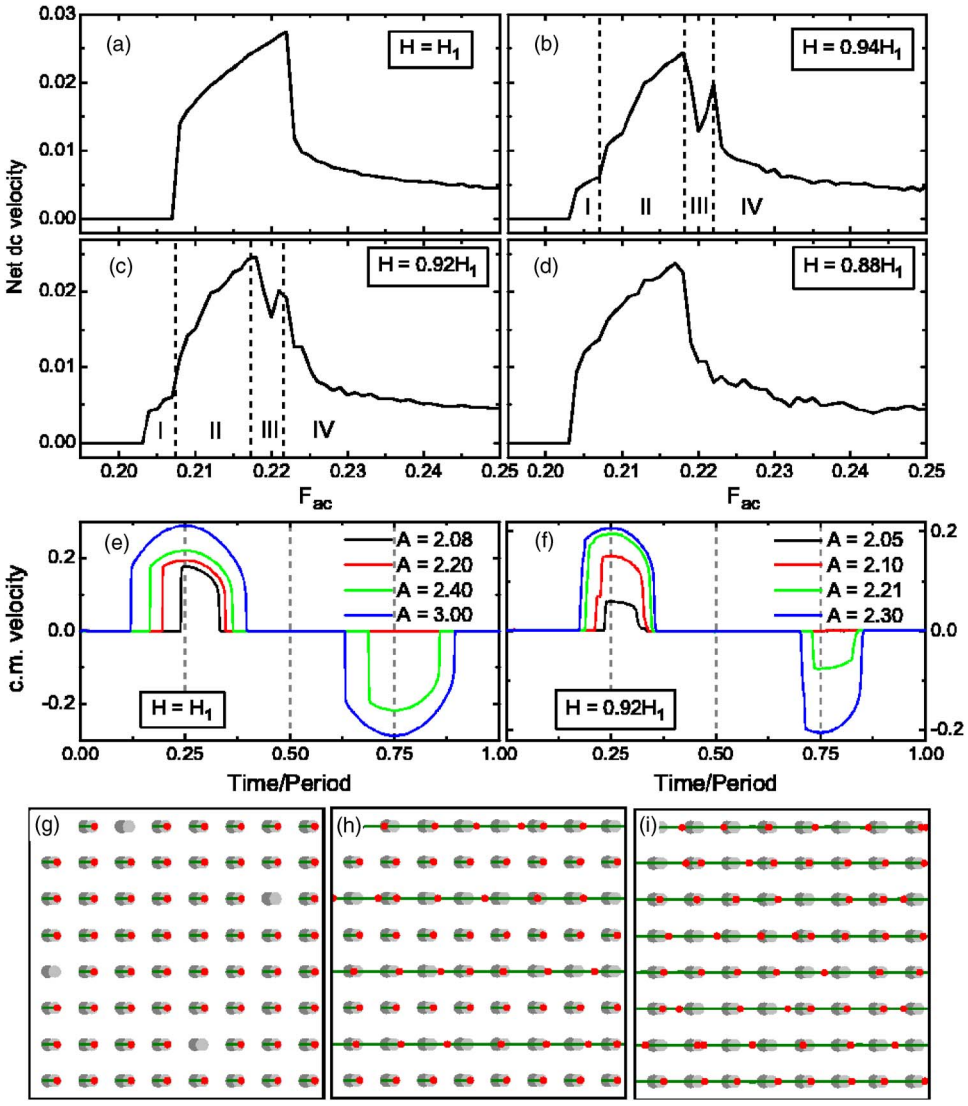

FIG. 8. (Color online) Molecular dynamics simulations results for $\eta=1$ and $M=1$. Panels (a)–(d): net dc velocity as a function of the ac driving force amplitude in normalized units (see text) at reduced fields $H/H_1=1$ (a), 0.94 (b), 0.92 (c), and 0.88 (d). The dashed lines in (c) and (d) define different dynamical regimes of the system (see text). Panels (e) and (f): time evolution of the c.m. velocity at $H/H_1=1$ (e) and 0.92 (f). Panels (g)–(i): vortex trajectories (lines) for $H/H_1=0.94$ at drive amplitudes 0.2 (g), where vortices are still pinned, 0.205 (h), where part of the vortices move as 1D channels, and 0.21 (i), where all vortices move. Vortices are represented by the small dots and the double pinning sites are represented by the asymmetric double disks.

lines in the V_{dc}-I_{ac} characteristic of Fig. 7(a) and in the $\langle v\rangle$-F_{ac} characteristics of Figs. 8(b) and 8(c)]. In phase I, only a fraction of vortices move in the easy direction of the pinning potential. No motion to the hard direction is observed. In phase II, the whole vortex lattice is half-wave rectified; i.e., all vortices move to the easy direction and no vortices move to the hard one. In phase III, we have motion of all vortices in the easy direction and motion of a fraction of them to the hard direction. The averaged rectified voltage drops abruptly at the onset of motion to the hard direction but increases again at slightly higher amplitudes, since the main ratchet (the whole vortex lattice) is still in its rectification window, giving rise to the second rectification peak. Finally, in phase IV, all vortices move back and forth, but in an asymmetric fashion, resulting in the long tail observed in the experiments and simulations.

To illustrate the interplay between the plastic dynamics and motion of the whole vortex lattice, we plotted in Figs. 8(g)–8(i) the vortex trajectories for the simulation at $H/H_1=0.94$ and a few drive amplitudes. At $F_{ac}=0.2$ (g), all vortices are still pinned (just oscillating inside the pinning centers). Note that, since the number of vortices does not match the number of pinning sites, there is a distribution of vacant pins—that is to say, of discommensurations in the vortex lattice. In this case and also for $H/H_1=0.92$, there are some vortex rows, with a denser distribution of discommensurations, which depin more easily. Thus, at $F_{ac}=0.205$ (h), only the weakly pinned vortex rows are dragged away, giving rise to a one-dimensional channeling dynamics characterized by a strong shear of the vortex lattice. Finally, at a higher drive $F_{ac}=0.210$ (i), the potential barriers for the strongly pinned vortex rows are also overcome and all vortices move to the easy direction of the pinning potential. At lower fields, such as $H/H_1=0.88$ shown in panel (d) of this figure, the distribution of vacancies is approximately homogeneous in such a way that all vortex rows have approximately the same depinning force. Thus, no channeling dynamics is observed and the $\langle v\rangle$-F_{ac} characteristic at this field presents a single rectification peak.

B. Vortex rectification for $H>H_1$

At fields higher than H_1, the interpretation of vortex motion in terms of underdamped dynamics may break down

because of the presence of interstitial vortices. Since they do not interact directly with the antidots, their dynamics is expected to be similar to that of vortices in a plain film—that is, essentially overdamped. This was indeed suggested by the amplitude dependence of the voltage wave forms $V(t)$ [see Figs. 4(g) and 4(h)]: whereas for high amplitudes the signal in a half-cycle is asymmetric, at lower amplitudes, the signal may be perfectly symmetric—that is, completely reversible. Since apparently hysteresis only comes out when the vortices trapped in the antidots are set into motion, one may then conclude that the apparent inertia comes from the interaction between vortices and antidots rather than from the real vortex mass.

V. CONCLUSION

In conclusion, we have studied the vortex ratchet effect in superconducting films with nanoengineered arrays of asymmetric and symmetric antidots. In the asymmetric antidot sample, we observed rectification of an unbiased ac current due to the intrinsic asymmetry of the system, thus demonstrating that this is an intrinsic vortex ratchet system. In the symmetric antidot sample, the rectification effect was due to the dc tilt of the periodic (symmetric) potential induced by the applied dc bias. The vortex rectification is strongly dependent on temperature and magnetic field. The temperature dependence indicates that the coherence length plays an important role in determining the effective asymmetry produced by the asymmetric antidot array; when the vortex size becomes comparable to the big antidot size, the rectification is strongly suppressed.

The field dependence of the rectification effects found in our experiments provides the following observations indicating collective behavior in the ratchet dynamics: (i) rectification is enhanced near the first matching field (cf. Fig. 2), evidencing the importance of vortex-vortex interactions in the ratchet effect (at the first matching field, the vortex-vortex interactions cancel out by symmetry); (ii) at some fields below H_1, a double-rectification peak was observed, which can be explained by the competition between rectification of (weakly pinned) incommensurate vortex rows and the rectification of the whole vortex lattice. If each vortex were rectified independently, such effects could never be observed. These effects result from the strong interaction between vortices. As has been demonstrated theoretically, independently moving particles shows a weaker ratchet effect as the number of particles increases, whereas when some interaction between them is turned on, particles may assist each other in a cooperative way, enhancing the ratchet effect.[26]

In addition, our data revealed that the ratchet effect for fields lower than H_1 is dominated by underdamped dynamics. These results were corroborated by molecular dynamics simulations of an underdamped vortex ratchet model. We argued that the inertial effect actually comes from vortex deformation due to the strong interaction with antidots, rather than from a finite vortex mass. Indeed, at fields higher than H_1, we observe that the dynamics of interstitial vortices is essentially overdamped, since these vortices are not pinned directly by the antidots.

ACKNOWLEDGMENT

We thank Alejandro Silhanek for useful discussions. This work was supported by the K.U.Leuven Research Fund GOA/2004/02 and FWO programs. C.C.S.S. is supported by CNPq, an Agency of the Brazilian Government. M.M. acknowledges support from the Institute for the Promotion of Innovation through Science and Technology in Flanders (IWT-Vlaanderen).

*Present address: Departamento de Física, Universidade Federal de Pernambuco, 50670-901, Recife, PE, Brasil.

†Present address: National Laboratory for Superconductivity, Institute of Physics, Chinese Academy of Sciences, Beijing 100080, China.

‡Electronic address: Victor.Moshchalkov@fys.kuleuven.ac.be

[1] M. O. Magnasco, Phys. Rev. Lett. **71**, 1477 (1993); **72**, 2656 (1994).

[2] For a review see P. Reimann, Phys. Rep. **361**, 57 (2002).

[3] Special issue: *Ratchets and Brownian Motors: Basic, Experiments and Applications*, edited by H. Linke, [Appl. Phys. A: Mater. Sci. Process.75, 167 (2002)].

[4] C. C. de Souza Silva and G. Carneiro, Phys. Rev. B **66**, 054514 (2002); in *Studies of High Temperature Supercondcutivity*, edited by A. Narlikar (NOVA Science, New York, 2005), Vol. 48, p. 71.

[5] A. V. Silhanek, L. Van Look, S. Raedts, R. Jonckheere, and V. V. Moshchalkov, Phys. Rev. B **68**, 214504 (2003).

[6] J. E. Villegas, E. M. Gonzalez, M. I. Montero, Ivan K. Schuller, and J. L. Vicent, Phys. Rev. B **68**, 224504 (2003).

[7] R. Wördenweber, P. Dymashevski, and V. R. Misko, Phys. Rev. B **69**, 184504 (2004).

[8] L. Van Look, E. Rosseel, M. J. Van Bael, K. Temst, V. V. Moshchalkov, and Y. Bruynseraede, Phys. Rev. B **60**, R6998 (1999).

[9] J. E. Villegas, S. Savel'ev, F. Nori, E. M. Gonzalez, J. V. Anguita, R. Garcia, and J. L. Vicent, Science **302**, 1188 (2003).

[10] J. Van de Vondel, C. C. de Souza Silva, B. Y. Zhu, M. Morelle, and V. V. Moshchalkov, Phys. Rev. Lett. **94**, 057003 (2005).

[11] C.-S. Lee, B. Jankó, I. Derényi, and A.-L. Barabási, Nature (London) **400**, 337 (1999).

[12] J. F. Wambaugh, C. Reichhardt, C. J. Olson, F. Marchesoni, and Franco Nori, Phys. Rev. Lett. **83**, 5106 (1999).

[13] C. J. Olson, C. Reichhardt, B. Jankó, and F. Nori, Phys. Rev. Lett. **87**, 177002 (2001).

[14] B. Y. Zhu, L. Van Look, V. V. Moshchalkov, B. R. Zhao, and Z. X. Zhao, Phys. Rev. B **64**, 012504 (2001); B. Y. Zhu, F. Marchesoni, V. V. Moshchalkov, and F. Nori, *ibid.* **68**, 014514 (2003).

[15] B. Y. Zhu, F. Marchesoni, and F. Nori, Phys. Rev. Lett. **92**, 180602 (2004).

[16] R. Bartussek *et al.*, Europhys. Lett. **28**, 459 (1994).
[17] G. Blatter, M. V. Feigel'man, V. B. Gehskenbein, A. I. Larkin, and V. M. Vinokur, Rev. Mod. Phys. **66**, 1125 (1994).
[18] B. N. J. Persson, Phys. Rev. Lett. **71**, 1212 (1993).
[19] K. H. Lee, Appl. Phys. Lett. **83**, 117 (2003).
[20] I. Zapata, R. Bartussek, F. Sols, and P. Hänggi, Phys. Rev. Lett. **77**, 2292 (1996); A. Sterck, S. Weiss, and D. Koelle, Appl. Phys. A: Mater. Sci. Process. **75**, 253 (2002).
[21] P. Jung, J. G. Kissner, and P. Hänggi, Phys. Rev. Lett. **76**, 3436 (1996).
[22] M. Borromeo, G. Costantini, and F. Marchesoni, Phys. Rev. E **65**, 041110 (2002).
[23] C. Reichhardt, C. J. Olson, and Franco Nori, Phys. Rev. B **58**, 6534 (1998).
[24] The first estimative of the vortex mass was given by Suhl [H. Suhl, Phys. Rev. Lett. **14**, 226 (1965)] in the framework of the time-dependent Ginzburg-Landau theory in the dirty limit. He estimated that the relaxation time $\tau = m_v/\eta$ of a vortex is typically 10^{-12} s. This means that collective vortex modes can only be excited at frequencies in the terahertz range, which is well beyond typical experimental conditions.
[25] D. J. Priour and H. A. Fertig, Phys. Rev. B **67**, 054504 (2003).
[26] I. Derényi and T. Vicseck, Phys. Rev. Lett. **75**, 374 (1995).